Power Flow Control of Bidirectional Modular Multilevel Resonant Converters in MVDC and LVDC Distribution Networks

Boliang Li, Jing Sheng, *Member, IEEE*, Long Xu, Tianling Shi, *Member, IEEE*, Shiyuan Fan, Xin Xiang, *Member, IEEE*, Xiaotian Zhang, *Senior Member, IEEE*, and Wuhua Li, *Senior Member, IEEE*

***Abstract*—This article proposes a bidirectional modular multilevel resonant dc converter (BMMRDC) and its power flow control strategy for medium-voltage dc to low-voltage dc distribution network First, a brief description of the BMMRDC topology structure is provided, followed by a detailed investigation of its operational principles under different operating modes. Then, the voltage gain model is studied, and the relationship between the transferred power and the operating frequency is precisely built. On this basis, a bidirectional power control strategy is proposed to adjust power flexibly by regulating the switching frequency. Furthermore, the soft-switching behaviors of the medium-voltage side and low-voltage side devices are analyzed to guide the parameter design of the converter, enabling soft-switching operation under a wide range of operating conditions. Finally, a downscaled BMMRDC prototype is constructed to validate the feasibility of the BMMRDC topology and the proposed control strategy.**

***Index Terms*—Bidirectional, modular multilevel resonant dc converters, power flow control, soft switching.**

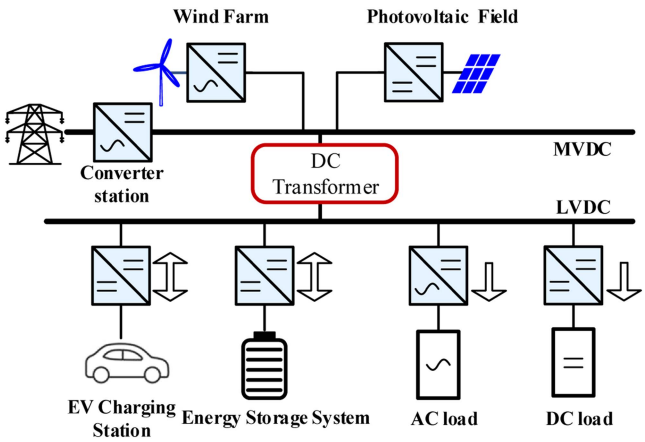

Fig. 1. DC distribution grid.

I. Introduction

In THE past two decades, the fast growth of renewable energy generation, energy storage, and electric vehicles has brought a variety of new dc sources [1], [2], dc storage [3], [4], and dc loads for the distribution networks [5], [6]. Compared with the ac system, the dc architecture has the good advantages of lower power losses, higher capacity, and improved stability to interconnect these dc components, as shown in Fig. 1, and the dc distribution networks become promising solutions in modern and future power systems [7], [8], [9].

The topology and control strategies of bidirectional dc–dc converters have been extensively studied and applied in the LV field [6], [11], [12]. Nonetheless, the insufficient blocking voltage of single-power devices would seriously affect their ability to withstand MV. Conventional LV topologies cannot extend to the MVDC field [12], [13], [14]. Although some solutions based on high-blocking-voltage devices have been proposed for dc converters, they are not suitable for large-scale commercialization due to their high price.

The mainstream approaches in the MV field include series connection of LV devices and series-parallel connection of LV converters [15], [16]. Series connection of devices provides advantages such as fewer switches and lower losses. However, during the transient process of turn-ON and turn-OFF, the dv/dt can reach tens of kV/μs, affecting the operational stability. Moreover, the voltage imbalance among series devices is another urgent problem in practical operation [17], [18]. The scheme based on the framework of LV converter modules with input series and output parallel connection has been widely applied in the MV field, which provides LV and power stress for modular design and manufacturing of single devices [19]. However, complex control strategies are essential for effectively addressing

Received 31 March 2024; revised 21 July 2024; accepted 11 September 2024. Date of publication 20 September 2024; date of current version 12 December 2024. This work was supported by the National Key Research and Development Program of China under Grant 2023YFB2407201. Recommended for publication by Associate Editor D. Dujic. *(Corresponding authors: Xin Xiang; Jing Sheng.)*

Boliang Li and Xiaotian Zhang are with the College of Electrical Engineering, Xi'an Jiaotong University, Xi'an 710049, China (e-mail: liboliang@stu.xjtu.edu.cn; xiaotian@xjtu.edu.cn).

Jing Sheng, Long Xu, Xin Xiang, and Wuhua Li are with the College of Electrical Engineering, Zhejiang University, Hangzhou 310027, China (e-mail: zjdxsj2013@zju.edu.cn; 22210071@zju.edu.cn; xiangxin@zju.edu.cn; woohualee@zju.edu.cn).

Tianling Shi is with the Shanghai Key Laboratory of Power Station Automation Technology, Department of Electrical Engineering, School of Mechatronics Engineering and Automation, Shanghai University, Shanghai 200444, China, and also with the School of Electrical and Data Engineering, University of Technology Sydney, Sydney, NSW 2007, Australia (e-mail: tianlingshi@shu.edu.cn).

Shiyuan Fan is with the Min H. Kao Department of Electrical Engineering and Computer Science, University of Tennessee, Knoxville, TN 37996 USA (e-mail: sfan8@utk.edu).

Color versions of one or more figures in this article are available at https://doi.org/10.1109/TPEL.2024.3465431.

Digital Object Identifier 10.1109/TPEL.2024.3465431

the voltage and current balancing challenges in the converter. Furthermore, the high-frequency transformers in each module pose obstacles to enhancing power density and efficiency [20], [21], [22].

Modular multilevel converters (MMC), which have achieved success in high-voltage power transfer systems, possess the advantages of flexible power control, high scalability, high efficiency, and high reliability [23]. The MMC-based dc–dc topologies have also attracted significant interest in MVDC distribution networks. The MMC was integrated with the dual active bridge (DAB) structure [24] to achieve bidirectional energy flow and incorporate voltage balancing in the modulation process [25]. However, the application of DAB faces large challenges due to the high current stress during the turn-OFF process and the limitations of operating frequency and transfer inductance on power transfer. This is particularly evident in cases of high step ratio, where the transfer inductance significantly limits the power of the converter.

The integration of the MMC with resonant converters offers an effective solution for mitigating switching losses by utilizing the leakage inductance of high turns ratio transformers as resonant inductors [26], [27]. This approach allows the converter to achieve power transfer that is not limited by transfer inductance. However, the presence of an uncontrollable diode rectifier limits bidirectional power flow [28]. To solve this problem, a converter structure with a series connection of single valves was proposed [29], but it functions similarly to the DAB topology and does not effectively address switching losses. An improved method was described in [30] to reduce losses by using resonant characteristics, but it mainly involves two unidirectional transfers and lacks the ability to continuously adjust the power flow direction in the converter.

To reduce device losses during power transfer in the converter and achieve bidirectional power transfer, a bidirectional modular multilevel resonant dc converter (BMMRDC) and its power flow control strategy are proposed in this article, where the MV side is composed of a series of submodules (SMs) and the LV side employs controllable switching devices. The gain of the *LLC* resonant network can be modified by adjusting the operating frequency, and thus the power flow can be flexibly changed between the MV side and LV side. Furthermore, the soft-switching characteristics of the converter and its boundary conditions are investigated in detail to guide the converter design. In this manner, the soft switching of devices in MV and LV sides can be achieved in the full power operating range.

The rest of this article is organized as follows. Section II introduces the circuit structure, modulation methods, and operational principles of the converter as a fundamental part of this article. Section III analyzes the gain expression of the converter and proposes the power flow control strategy. Then, the soft switching of the converter is investigated to guide the design of circuit parameters for efficient operation. In Section IV, the feasibility of the proposed control strategy and the soft-switching characteristics of the device are verified by simulation, and a 4.5-kW downscaled prototype is built for experimental verification. Finally, Section V concludes this article.

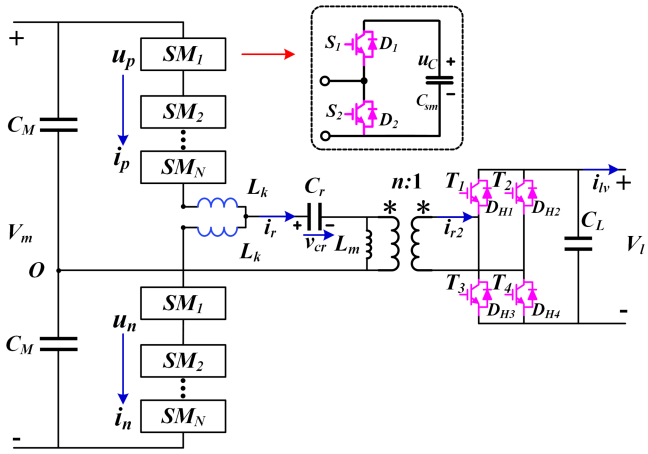

Fig. 2. Bidirectional modular multilevel resonant DC–DC converter.

II. Fundamentals of Proposed BMMRDC

A. BMMRDC Topology

As shown in Fig. 2, the BMMRDC consists of three parts: the MMC converter, the resonant structure, and the secondary-side rectifier. The medium-voltage side of BMMRDC topology is composed of split capacitors and two stacks of SMs that replace switching devices of the traditional half-bridge resonant converter, which facilitates the conversion of MVDC to ac and it has the combination advantages of modular multilevel circuits and *LLC* resonant converters. The composition of each stack remains constant, including N SMs and arm inductors L_k. Besides, L_r is the resonant inductance which is composed of the arm inductor and the transformer leakage inductor. The resonant unit consists of the resonant inductor, resonant capacitor C_r, and excitation inductor of the transformer L_m. Besides, the transformer ratio is n. The secondary side of the transformer is connected to the H-bridge as a controllable rectifier. In addition, the full-bridge structure composed of IGBTs on the secondary side of the transformer can achieve bidirectional power transfer. Compared with the H-bridge type or three-phase type MMC, the half-bridge MMC structure can significantly save the number of SMs by more than half, and thus reduce the switching devices, circuit cost, and operation losses. The split dc capacitors are installed to absorb the high-frequency current ripple, and thanks to the high operation frequency, such as 10 kHz, the dc capacitance is much smaller than that in the 50-Hz systems with the same power rating. Similar to the conventional *LLC* resonant converter, the BMMRDC possesses two resonance frequencies given as follows:

$$f_r = \frac{1}{2\pi\sqrt{C_r L_r}} \tag{1}$$

$$f_m = \frac{1}{2\pi\sqrt{C_r\left(L_r + L_m\right)}} \tag{2}$$

where the operation frequency is designed between f_m and f_r to ensure the inductive impedance of the resonant unit.

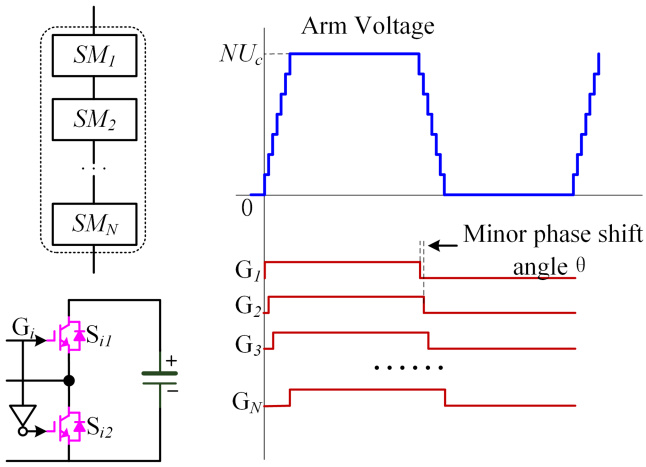

Fig. 3. Quasi-square wave modulation of the BMMRDC converter.

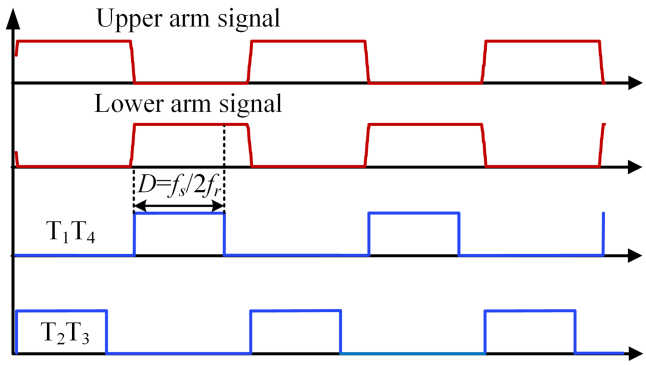

Fig. 4. Control signal of the BMMRDC converter.

The quasi-square wave modulation method can achieve a high voltage utilization and mitigate the high dv/dt on the transformer and devices [31]. The quasi-square wave can be easily generated by utilizing a small phase shift angle among the SMs switching signals, as shown in Fig. 3. Meanwhile, the LV-side H-bridge is driven by a signal with a specific duty cycle D, defined as $D = f_r/2f_s$ and f_s is the operating frequency. The control signals of the MMC unit and the H-bridge module are shown in Fig. 4. The duty cycle D varies only depending on the operating frequency f_s of the converter and is positively correlated, but always less than 0.5. When all SMs are inserted in the upper arm, the secondary-side switches T_1 and T_4 are turned ON. Similarly, when the lower arm SMs are engaged, T_2 and T_3 are turned ON.

Generally, the high-frequency operation can reduce the volume and weight of passive elements and improve the system power density. In the MVDC to LVDC conversion system, the voltage step ratio is very large, such as 10 kV to 400 V, where the leakage inductance of the transformer would be large. Hence, it is better to configure the converter work in resonant mode to utilize the large leakage inductance, rather than the DAB structure. Meanwhile, as the rated frequency increases, the dimensions of the high-frequency transformer will decrease. To simplify the analysis, the rise and fall processes of the arm voltage are approximated as linear diagonals. The rest of the assumptions are as follows.

1) All components are assumed to be ideal.
2) The terminal voltage of LV and MV remains stable.
3) The capacitances of SMs are uniform and the inductance of both arms remains equal.

The assumption that all devices may be treated as ideal cases ignores the effect of parasitic parameters of devices on the analysis, as well as the impact of changes in the values of passive components due to current variations. To consider all the SMs as identical states, the capacitance of SMs is required to be identical and SMs have no voltage ripples.

B. Operation Mode

The BMMRDC can be categorized into three modes determined by the direction and magnitude of transfer power: forward mode, zero power mode, and reverse mode, as shown in Fig. 5(a)–(c), respectively. Forward transfer power is defined as the power flow from the MV side to the LV side. The transfer power increases by decreasing the switching frequency. At low operating frequencies, the secondary-side rectifier unit operates similarly to a synchronous rectifier. As the operating frequency of the BMMRDC increases, the transfer power of the converter decreases. When the switching frequency is increased beyond a certain value, the transferred power becomes negative. Then, the BMMRDC automatically enters reverse mode, where the power is from the LV side to the MV side.

1) Forward Operating Mode. Mode 1[t_0–t_3]: MMC SMs switching completes at t_0. Then, the equivalent voltage on the MV side is $0.5V_m$, whereas the voltage on the LV side is V_l. The primary current starts to resonate, and the excitation current linearly increases simultaneously. The currents in the upper and lower arms reverse their directions at t_1 and t_2, respectively. The lower switches of the upper arm SMs and the upper switches of the lower arm SMs realize zero-voltage switching (ZVS) turn-ON. This mode continues until t_3 when the primary current is equal to the excitation current. In this mode, the state equation of the circuit can be written as

$$\begin{cases} C_r \frac{dv_{cr}(t)}{dt} = i_r(t) \\ L_r \frac{di_r(t)}{dt} = \frac{1}{2}V_m - v_{cr}(t) - nV_l \end{cases} \tag{3}$$

where v_{cr} is the voltage of the resonant capacitor and i_r is the primary current.

Mode 2[t_3–t_4]: At t_3, the primary current is equal to the excitation current and L_m starts to involve the resonance, resulting in zero current flow on the secondary side of the transformer. The current in the H-bridge is zero, allowing the zero-current switching (ZCS) of the devices to turn OFF. The state equation of the circuit in this mode can be expressed as

$$\begin{cases} C_r \frac{dv_{cr}(t)}{dt} = i_r(t) \\ (L_r + L_m) \frac{di_r(t)}{dt} = \frac{1}{2}V_m - v_{cr}(t) \end{cases}. \tag{4}$$

Mode 3[t_4–t_5]: At t_4, the working state of the upper and lower arms are exchanged. The SMs of the upper arm are inserted and the SMs of the lower arm is bypassed. The equivalent voltage on the MV side begins to decrease until it reaches 0.5 V_m.

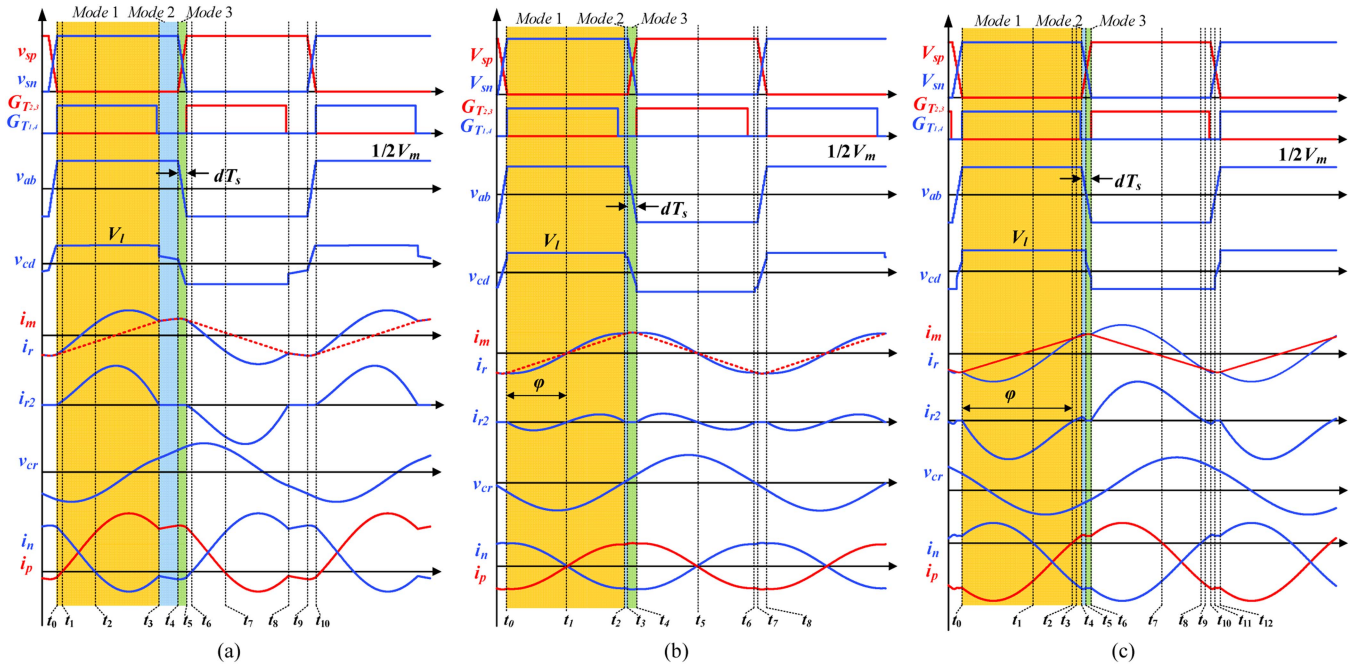

Fig. 5. Key operational waveforms of the BMMRDC in three operating modes. (a) Forward operating mode. (b) Zero power operating mode. (c) Reverse operating mode.

Simultaneously, there is no current flow on the secondary side throughout the entire mode. In this mode, the state equation of the circuit can be written as

$$\begin{cases} C_r \frac{dv_{cr}(t)}{dt} = i_r(t) \\ (L_r + L_m) \frac{di_r(t)}{dt} = \frac{1}{2}V_m - \frac{V_m}{dT_s}(t - t_4) - v_{cr}(t) \end{cases}. \quad (5)$$

Hence, the analysis of the operating principle for the first-half cycle has been finished and the same analysis approach can be applied to the rest of the period. The proposed BMMRDC maintains a positive power transfer throughout the complete cycle.

2) Zero Power Operating Mode. Mode 1[t_0–t_2]: The converter initiates resonance at t_0. The gain of the resonant network is influenced by the operating frequency. At the start of the period, a negative resonant current is generated that is lower than the excitation current. Energy transfers from the LV side to the MV side. At t_1, the devices of SMs achieve ZVS. Then, the resonant current reverses, causing the secondary side current to flow through the diode and enabling the reverse flow of energy. In this mode, the state equation of the circuit also can be written as (3).

Mode 2[t_2–t_3]: At t_2, the resonant current gradually decreases while the excitation current increases. Eventually, they become equal, achieving ZCS turn-OFF of diodes D_{H1} and D_{H4} in the H-bridge. In this mode, the state equation of the circuit is the same as in (4).

Mode 3[t_3–t_4]: The equivalent voltage at the MV level shifts from $0.5V_m$ to $-0.5V_m$, finishing the upper and lower arms switching process. During t_3–t_4, the secondary side current keeps at zero, and no energy is delivered. The state equation of the circuit in this mode can be expressed as

$$\begin{cases} C_r \frac{dv_{cr}(t)}{dt} = i_r(t) \\ (L_r + L_m) \frac{di_r(t)}{dt} = \frac{1}{2}V_m - \frac{V_m}{dT_s}(t - t_3) - v_{cr}(t) \end{cases} \quad (6)$$

where d represents the percentage of the arm alternation time and T_s is the resonant period.

The power transfer magnitude depends on the gain of the resonant unit. During the time interval from t_0 to t_1, the energy flow direction is negative. Then, the energy flow direction is reversed between t_0 and t_1. The converter is in current discontinuity mode from time t_1 to t_2 and the energy does not flow through the converter. At a specific operating frequency, the energy transmitted in both directions is equal, indicating no transfer of power between the MV side and the LV side.

3) Reverse Operating Mode: Mode 1[t_0–t_4]: At t_0, similar to the previous analysis, the arm SMs switching is completed and resonance is initiated. The currents in the two arms are, respectively, reversed at t_1 and t_2 to achieve the ZVS of the device of the SMs. At t_3, the resonant current exceeds the excitation current, causing a change in the current on the secondary side. The current on the secondary side increases before alternating the upper and lower arms. During t_0–t_4, the BMMRDC only transfers reverse energy.

Mode 2[t_4–t_5]: After t_4, the equivalent voltage of the modular multilevel circuit begins to decrease linearly. The primary current decreases as the equivalent input voltage of the resonant unit falls, until it reaches the value of the excitation current, with a slope of $-V_m/dT_s$. The state equation of the circuit can

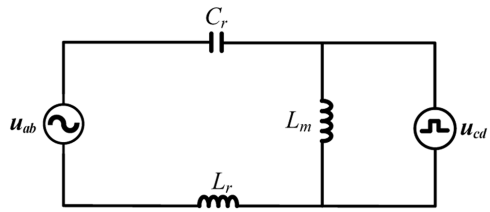

Fig. 6. Steady-state equivalent circuit of the BMMRDC.

be written as

$$\begin{cases} C_r \frac{dv_{cr}(t)}{dt} = i_r(t) \\ (L_r + L_m) \frac{di_r(t)}{dt} = \frac{1}{2} V_m - \frac{V_m}{dT_s}(t - t_3) - v_{cr}(t) \end{cases}. \quad (7)$$

Mode 3[t_5–t_6]: The primary current is equal to the excitation current, and thus the excitation inductance participates in resonance. At t_5, the secondary current flowing through the diode of T_2 and T_3 is reduced to zero to achieve the ZCS OFF. Until t_6, the upper and lower arms complete the switching process, which represents the end of this mode. In this mode, The circuit's state equation is expressed as follows:

$$\begin{cases} C_r \frac{dv_{cr}(t)}{dt} = i_r(t) \\ L_r \frac{di_r(t)}{dt} = \frac{1}{2} V_m - \frac{V_m}{dT_s}(t - t_4) - v_{cr}(t). \end{cases} \quad (8)$$

According to the analysis mentioned above, the physical quantities of the converter in different modes have been determined. The soft-switching behavior of the device in the SM occurs when the direction of the arm current changes and that in the H-bridge happens due to the secondary side current being zero. As the operating frequency increases, the reverse energy also increases.

III. Proposed Power Flow Control of BMMRDC

A. Proposed Power Flow Control

The steady-state equivalent circuit of the BMMRDC is shown in Fig. 6. The fundamental component method is widely employed for circuit analysis [32], which can simplify both the inverter and rectifier sections.

In the forward operation mode, it operates similarly to a unidirectional resonant converter. In this mode, the LV source acts as an external load, representing the actual power of the converter. By applying the fundamental wave to the analysis, the gain expressions for the low and medium voltage sides can be derived through the fundamental principles of circuit analysis. When the LV side current I_{lv}>0, the relationship between the operation frequency and the quality factor of the BMMRDC is given as follows:

$$\frac{2nV_l}{V_m} = \frac{1}{\sqrt{\left(1 + \frac{1}{k} - \frac{1}{kf_n^2}\right)^2 + Q^2\left(f_n - \frac{1}{f_n}\right)^2}} \quad (9)$$

$$f_n = f_s / f_r \quad (10)$$

where f_n refers to the equivalent frequency, k is the inductance ratio, and Q is the quality factor that is defined as follows:

$$Q = \frac{\pi^2 I_{lv} \sqrt{L_r / C_r}}{8n^2 V_l} \quad (11)$$

$$k = L_m / L_r. \quad (12)$$

Power is determined by the current while keeping the voltage constant on both the MV side and the LV side. The essence of the method is to change the equivalent impedance on the LV side, resulting in a change in the transferred power. The voltage gain is maintained at a constant level, whereas the converter power is regulated by adjusting the gain of the resonant unit. A positive correlation exists between the current on the LV side and the quality factor Q, as shown in (11). Consequently, once the converter operates under a light-load condition, the energy backflow occurs. The expression (9) requires further analysis to derive the gain expression.

The phase angle between voltage and current on the secondary side of the transformer is no longer consistent under light-load situations. This is due to a change in the gain of the resonant unit, which results in a shift in the equivalent load on the low-voltage side from resistance to impedance. During the half period, the amplitude of the resonance current is no longer always larger than the amplitude of the excitation current. The direction of the secondary current will be negative at first. Then, the direction of the current changes to positive. The power direction and magnitude of the total converter are determined by the net value of positive energy and negative energy. The expression for the equivalent impedance Z_e is given as

$$Z_e = \frac{u_{cd}}{i_{cd}} = \frac{8n^2 V_l \cos\varphi}{I_{lv}\pi^2} \angle\varphi \quad (13)$$

where u_{cd} and i_{cd} are the fundamental wave component of the secondary side voltage and current, respectively. The phase shift angle φ represents the phase angle difference between the secondary voltage and current. The expression for the power factor angle of Z_e is a transcendental equation [11], which cannot obtain an analytical expression and the numerical results are calculated with specific parameters.

Similarly, the gain in this mode can be obtained from the relationship of the equivalent circuit as follows:

$$H(j\omega) = \frac{Z_e || j\omega L_m}{n^2 Z_e || j\omega L_m + j\omega L_r + \frac{1}{j\omega C_r}}. \quad (14)$$

Thus, the relationship between the equivalent impedance, which is determined by quality factor Q, and the operating frequency can be developed as (15). It is noted that the power shift angle φ is dependent on the *LLC* resonant unit parameter, power flow, and operating frequency.

When the power shift angle φ is zero, the power is always transmitted from MV to LV, which is consistent with (9). When the power shift angle φ is in the range of 0°–90°, the converter can still maintain the direction of the power flow positive. As the power shift angle further increases between 90° and 180°, the direction of power flow changes to negative. Thus, the power shift angle φ affects the direction of the power flow. Adjusting

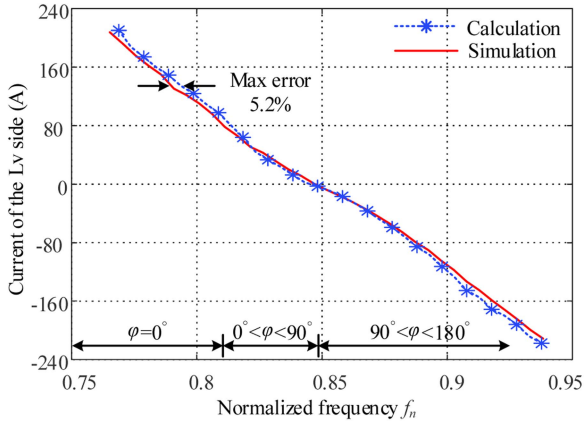

Fig. 7. LV-side current versus f_s when $L_r = 1.45$ mH, $C_r = 119$ nF, and $k = 5$.

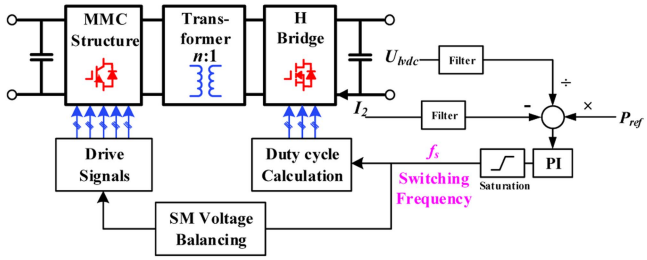

Fig. 8. Control block diagram of BMMRDC.

the power shift angle essentially means adjusting the switching frequency.

The relationship between the secondary current and the normalized operation frequency is clearly shown in Fig. 7. As a consequence of the variation of the operating frequency, the operational mode of the converter undergoes a corresponding change, thus, it becomes necessary to make use of (12) and (15) shown at the bottom of the this page, to ascertain the theoretical value of the LV-side current. The operational conditions are 10 kV on the MVDC and 400 V on the LVDC, respectively. Furthermore, the resonant inductance is 1.45 mH, the resonant capacitance is 119 nF, and the inductance coefficient k is 5. The BMMRDC can operate flexibly in both forward and reverse modes by adjusting the switching frequency. The two curves are the theoretical calculations of the modeling and the simulation results, respectively. The difference between the calculation and simulation results is mainly due to the neglect of the high-frequency component in the modeling process. In addition, the maximum error between the simulation and the calculation is only 5.2%. Consistent with theoretical analysis, as the operation frequency increases, the power transfer behavior of the converter is affected, which is approximately linear to the operation frequency.

Effective control of the converter is essential to ensure its stable operation and regulated power transfer. The control strategy plays a pivotal role in the system. Fig. 8 shows the proposed structural diagram of the power control strategy. The controllable elements consist of the MMC unit and H-bridge unit with synchronized control timers.

In the above analysis, a mathematical model between the transferred power of the converter, operating frequency, and power shift angle is obtained, based on which a control strategy for power flow can be obtained. As shown in Fig. 8, the switching frequency of the converter can be determined through a proportional-integral regulator by comparing the power reference $P_{\rm ref}$ with the output voltage $U_{\rm lvdc}$ and current I_2. The voltage and current can be also measured from the MV side. To ensure the stable operation of the converter, the operating frequency obtained by the controller needs to be limited within the desired range. The duty cycle for the H-bridge can be calculated according to the resonant frequency and operating frequency. Then, voltage balancing among capacitors of the SM is achieved through a voltage balancing algorithm in modular multilevel units.

B. Soft-Switching Analysis

All the devices in the LV-side full bridge can achieve the ZCS with appropriate parameter design and the mentioned modulation strategies. In the half-bridge SM on the MV side, the currents of the arm can be divided into a dc component and an ac component. Then, the upper and lower arm currents i_p and i_n can be expressed as

$$\begin{cases} i_p = \frac{1}{2} i_r + i_{\rm dc} \\ i_n = -\frac{1}{2} i_r + i_{\rm dc} \end{cases} \tag{16}$$

where $i_{\rm dc}$ is the ac component of the string current.

1) Soft Switching of the Half-Bridge SMs: When the SMs are inserted one by one if the arm current direction is positive, the current will flow from the switch S_2 to the diode D_1, where S_2 is the IGBT of the lower device in the SM and D_1 is the diode of the upper device. Hence, the voltage of S_1 which is the IGBT of the upper device in the SM decreases to zero to facilitate ZVS-ON, as shown in Fig. 9(a). Similarly, when the SMs are bypassed from the inserted status, if the arm current direction is negative, the current will flow from switch S_1 to diode D_2 which is the diode of the lower device. It means the voltage of S_1 is zero at the string current changing direction to realize ZVS-ON, as shown in Fig. 9(b).

The ability of SM devices to achieve soft switching is determined by the arm current direction of the switching point, which is different from the *LLC* converter. Under heavy load conditions, the possibility of soft switching would be lost due to the large dc bias current, as shown in Fig. 10. The high amplitude of

$$\frac{2nV_l}{V_m} = \frac{1}{\sqrt{\left(1+\frac{1}{k}-\frac{1}{kf_n^2}\right)^2 + 2Q\tan\varphi\left(f_n-\frac{1}{f_n}\right)\left(1+\frac{1}{k}-\frac{1}{kf_n}\right) + \left[\frac{Q}{\cos\varphi}\left(f_n-\frac{1}{f_n}\right)\right]^2}}. \tag{15}$$

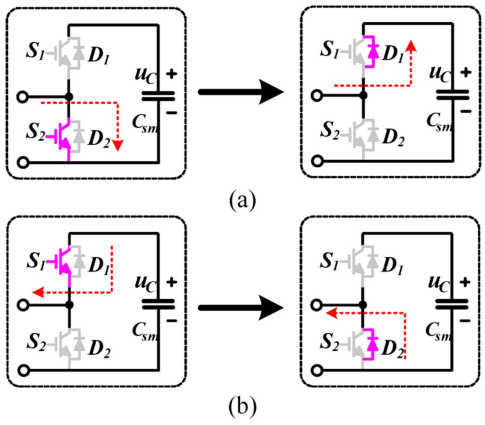

Fig. 9. Switching description of the inserted and bypassed states. (a) Inserted. (b) Bypassed.

the dc component is responsible for the failure of soft switching in both forward and reverse modes. However, it is worth noting that in the light load condition shown in Fig. 10, both transfer modes exhibit favorable soft-switching behaviors. Fig. 11 shows the arm currents at different switching instances corresponding to various inductance ratios under power operating conditions ranging from −80 to 80 kW.

The soft-switching behaviors are related to the dc bias and excitation current i_m. Thus, the specific expression for the relationship between the two currents is as follows:

$$|i_{\rm dc}| < \frac{1}{2}|i_{m,\rm amp}| \tag{17}$$

where $i_{m,\rm amp}$ is the amplitude of the excitation current, which is related to the voltage of excitation inductance and its value as described in the following equation:

$$i_{m,\rm amp} = \frac{nV_l}{4L_m f_s}. \tag{18}$$

The dc component $i_{\rm dc}$ can be calculated from the transferred power and voltage.

The excitation current is determined by the excitation inductance, based on (17), and (18), so the boundary expression for achieving soft switching, under maximum power operating conditions can be expressed as follows:

$$\frac{nV_mV_l}{8Pf_s} > L_m. \tag{19}$$

2) Soft Switching for the LV-Side H-Bridges: The steady-state waveform diagram of the operation has been previously discussed above. During positive power operation, the current flows through the antiparallel diode, which means the soft switching of the device can be achieved.

As shown in Fig. 5, the soft-switching behavior would be achieved if the secondary current i_{r2} is reduced to zero during the arm alternating period in reverse operation. Before the end of the half period, reducing the secondary current i_{r2} to zero, the device in the H-bridge can obtain ZCS. Therefore, the following

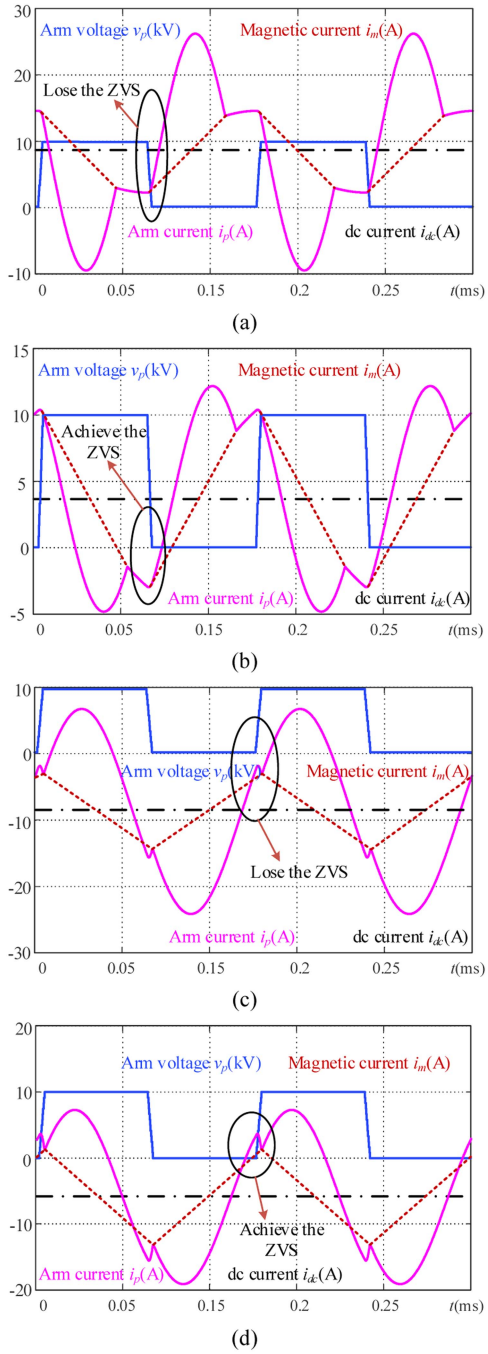

Fig. 10. Operation waveforms of the MMC unit. (a) SMs lose ZVS in forward mode. (b) SMs achieve ZVS in forward mode. (c) SMs lose ZVS in reverse mode. (d) SMs achieve ZVS in reverse mode.

equation should be satisfied:

$$\frac{T_s}{2} - t_5 > 0. \tag{20}$$

The losses of the device are calculated based on its parameters, which are divided into conduction and switching losses for SM devices and conduction losses for H-bridge devices. Thus, the calculation expression is shown in the following equation:

$$P_{\rm loss} = P_{\rm SM,con} + P_{\rm SM,}{}_{sw} + P_{H,\rm con}. \tag{21}$$

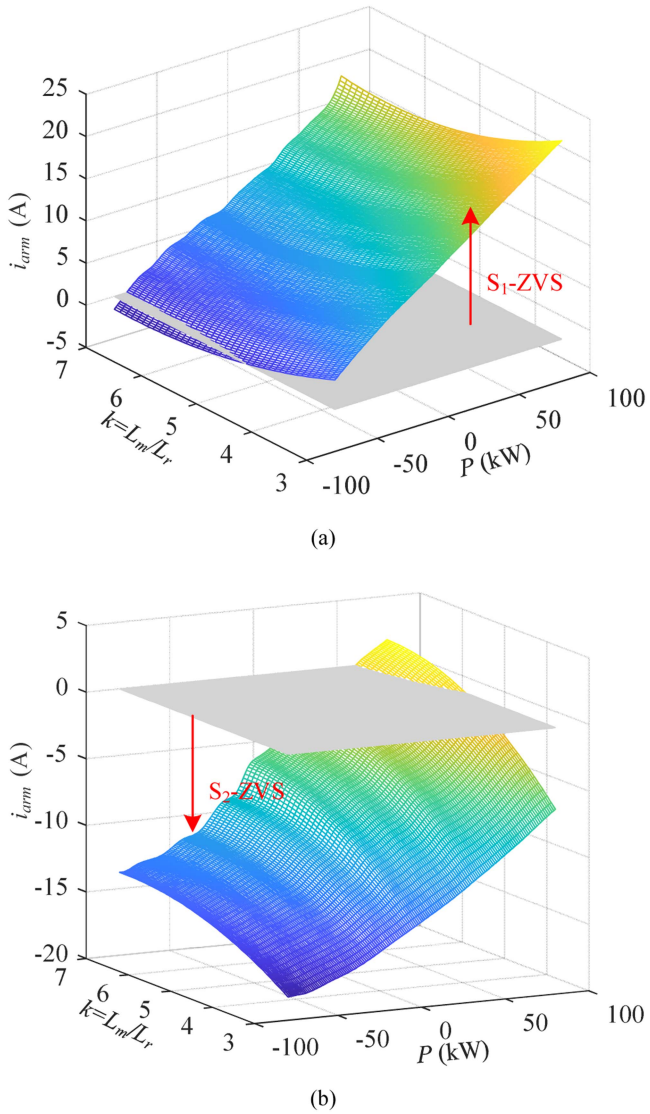

Fig. 11. Situation of the SMs switching devices achieving soft switching under different power and inductance ratios. (a) Upper devices of the SM. (b) Lower devices of the SM.

Besides, the switching devices have a voltage drop during conduction and have switching losses related to the voltage and current.

The previous section discussed the composition of device losses in the MMC unit. Thus, soft-switching behavior can be achieved by optimizing the circuit parameters, but it is still challenging to avoid losses during device turn-OFF. The arm current flows through two paths, the IGBT and the diode. Nevertheless, the current is sustained on these two elements for disparate periods, thereby giving rise to losses associated with the duration of the current. Therefore, the expressions for the device of the MMC unit and H-bridge are provided as

$$P_{\mathrm{SM,con}} = P_{S,\mathrm{con}} + P_{D,\mathrm{con}} = 2\alpha N V_T I_{\mathrm{arm}} + 2(1-\alpha) N V_F I_{\mathrm{arm}} \tag{22}$$

$$P_{\mathrm{SM},sw} = P_{S,sw} = 4N f_s E_{T,\mathrm{OFF}}(I_{\mathrm{arm}}, U_c) \tag{23}$$

where I_{arm} is the average value of the arm current, α represents the duration of the current flowing through the IGBT, V_T and V_F can be found in the datasheet, and $E_{T,\ \mathrm{OFF}}$ is the element about turn-OFF losses of IGBT. Power flows through the diode during the forward operation, resulting in losses, given as

$$P_{H,\mathrm{con}} = 4 V_F I_{r2} \tag{24}$$

where I_{r2} is the root mean square (RMS) of the secondary current.

The main loss difference between reverse and forward mode is the distribution of device losses in the H-bridge. The device still maintains the ZCS behavior. However, the current passes through both the IGBT and the diode in one period. The losses generated by diodes and IGBTs are related to the power shift angle φ, which influences the duration time of current flow through IGBT. Thus, the conduction losses are the sum of the losses of both devices. The expression is presented as

$$P'_{H,\mathrm{con}} = 2\frac{\pi-\varphi}{\pi} V_F I_{r2} + 2\frac{\varphi}{\pi} V_T I_{r2}. \tag{25}$$

Device losses play a crucial role in the overall efficiency losses. Calculate the efficiency losses caused by the device at 80 kW power transfer, excluding losses due to parasitic parameters and transformer effects, the efficiency of the forward mode and the reverse mode has been determined to be 98.1% and 97.9%, respectively. Due to the energy backflow, the efficiency in reverse mode is less than in forward mode.

C. Design of the LLC Resonant Unit

The resonant unit must operate in the inductive region to achieve the soft-switching behavior of the H-bridge circuit. If the resonant network has a purely resistive characteristic, then the network is located at the boundary between the inductive and the capacitive regions. Hence, this is the maximum quality factor that ensures the resonant unit works in the inductive region. The expression relating the quality factor and the normalized frequency is given as follows:

$$Q_z(k, f_n) = \sqrt{\frac{1}{k + k f_n^2} - \left(\frac{1}{k f_n}\right)^2}. \tag{26}$$

When operating at the boundary of the resonant unit impedance characteristic, the relationship between the minimum operating frequency, voltage gain, and inductance ratio is given in the following equation:

$$f_{n,\min} = \sqrt{\frac{1}{1 + k\left(1 - \left(\frac{V_m}{2nV_l}\right)^2\right)}}. \tag{27}$$

The expression given in (27) can be used to determine the minimum operating frequency $f_{n,\min}$ of the converter. Using the equation for the quality factor, the parameters of the resonant unit can be calculated by an iterative method.

Fig. 12 shows the procedure of the parameter design for the resonant unit. First, the ratio of the transformer and resonant frequency are determined. The inductance ratio k is typically chosen between 3 and 8. Then, the maximum

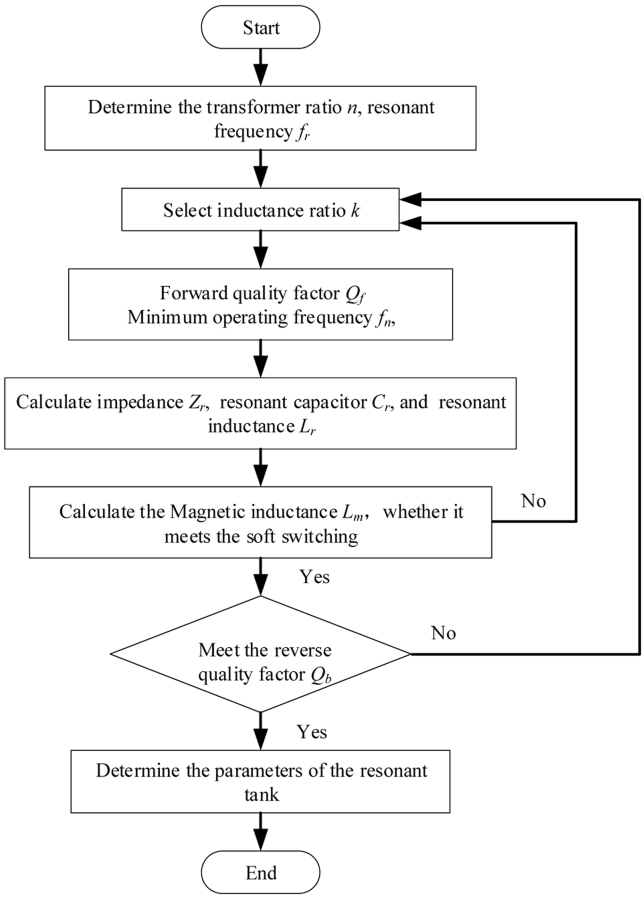

Fig. 12. Program diagram for transformer parameter design.

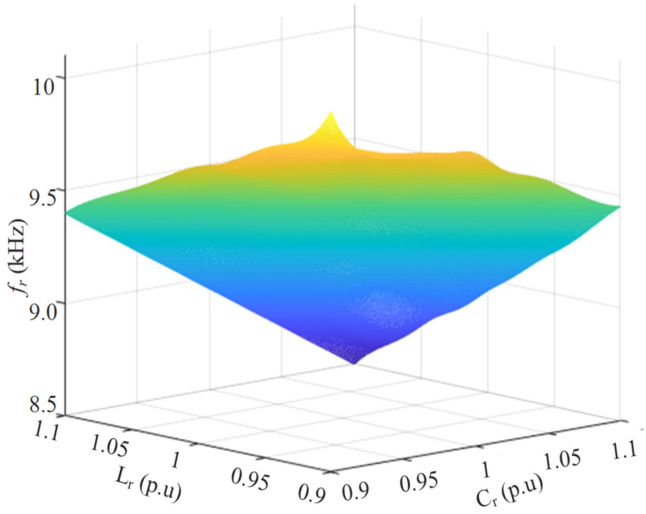

Fig. 13. 3-D diagram of the effect of resonance parameters on operating frequency.

TABLE I
COMPARISON RESULTS OF DIFFERENT SCHEMES

	Power bidirectional	Continuous power control	Range of soft-switching
Method in [26]	No	—	Large
Method in [30]	Yes	No	Large
Method in [34]	Yes	Yes	Small
Proposal method	Yes	Yes	Large

quality factor Q is calculated according to (26). Furthermore, the resonant capacitance and resonant inductance are then determined by the maximum transmitted power and the equivalent impedance. The validity of the parameter is assessed by examining its soft-switching behavior in forward mode. If the soft-switching behavior is satisfied, the subsequent steps are executed. Otherwise, a new inductance ratio should be tuned again. Finally, it is verified whether the maximum transfer power can be transmitted in the reverse transfer mode.

The circuit parameters exert influence on the power regulation of the converter, particularly regarding the passive components of the resonant unit. The 3-D plot of the variation of the operating frequency for a 10% fluctuation in the values of the resonant parameters is plotted at the maximum transmitted power, as shown in Fig. 13. An increase in the parameter results in a reduction in the operating frequency due to a decrease in the resonant frequency and vice versa. Furthermore, an increase in the parameter also affects the gain of the resonant unit. To maintain a constant voltage gain, it is necessary to reduce the operating frequency. A 20% change in capacitance value is the end-of-life of the device. However, in practice, the limit for the end-of-life of the capacitor is a 10% change in value, considering the overall reliability of the application [33].

D. Comparison With Different Control Strategies

In this section, a thorough comparison is conducted among the control strategy in [26], [30], and [34] and the proposed strategy. The comparison is performed in terms of the power bidirectional, the continuous power control, and the range of the soft switching. Considering the performance and cost of existing commercial devices, the IKW40N120CS6 and FF450R12ME4 semiconductor switches are chosen as the power switches for MV side SMs and LV side H-bridge for the converter, respectively.

The converter has different power transfer characteristics under different control strategies, summarized in Table I. It can be obtained that the approach proposed in [26] does not support bidirectional power transfer, and the method used in [30] requires changing the control strategy when the power is reversed. Therefore, it would be difficult to continuously control the transferred power, and the control scheme in [34] has a small soft-switching range, which could make the device loss severe. The control strategy proposed in this article could perform better in these dimensions.

The device losses are calculated under the 10 kV/80 kW operating conditions with the control strategies in [30] and [34] and the method in this article, respectively, as shown in Fig. 14. The soft-switching behavior over a wider operating range can reduce the switching losses by more than 50%, whereas the reduction of the arm RMS current during operation further reduces the conduction losses.

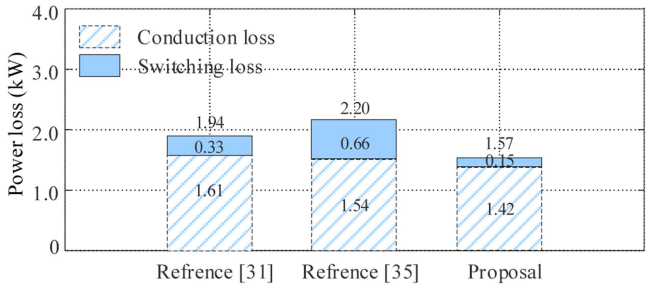

Fig. 14. Power losses breakdown of three schemes.

TABLE II
PARAMETERS OF SIMULATION

Parameters	Value
Medium terminal voltage V_m	10 kV
Low terminal voltage V_l	400 V
Bidirectional power P_{max}	±80 kW
MMC arm SM number N	12
SM capacitance C_{sm}	60 μF
Resonant ratio k	5
Transformer turns ratio n	13:1
Resonant frequency f_r	12 kHz
Resonant capacitor C_r	119 nF
Resonant inductance L_r	1.45 mH
Switching frequency f_s	9–12 kHz
SM switching devices	IKW40N120CS6 1200 V/40 A
H bridge devices	FF450R12ME4 1200 V/450 A

IV. SIMULATION AND EXPERIMENT.

A. Simulation Results

A simulation of the BMMRDC is constructed in the PLECS platform to demonstrate the effectiveness of the proposed control strategy and parameter design. The circuit parameters are provided in Table II. The voltage of the MV side is 10 kV, the voltage of the LV side is 400 V, and the maximum bidirectional power is 80 kW.

To simplify the analysis, the power switches and passive components are assumed to be ideal. Fig. 15 shows the steady-state operation waveform of the converter, including the voltage and current of the arm and primary current. Fig. 15(a) and (b) shows the operating waveforms at 80 kW and −80 kW, respectively. Under the 80-kW load condition, the dc component of the arm is positive. Taking the upper arm as an example, keeping the arm current negative at the switching point of the arm can ensure the lower side switches of the SMs achieve ZVS-ON when the SM is bypassed.

The operation at maximum transfer power satisfies the soft-switching condition for the entire forward mode. This is confirmed by the relationship between the arm voltage and current shown in Fig. 15(a). Furthermore, it should be noted that the resonance current and excitation current are equal every half period. This indicates that the current in the H-bridge device is zero during they are turned OFF, which ensures the ZCS-OFF

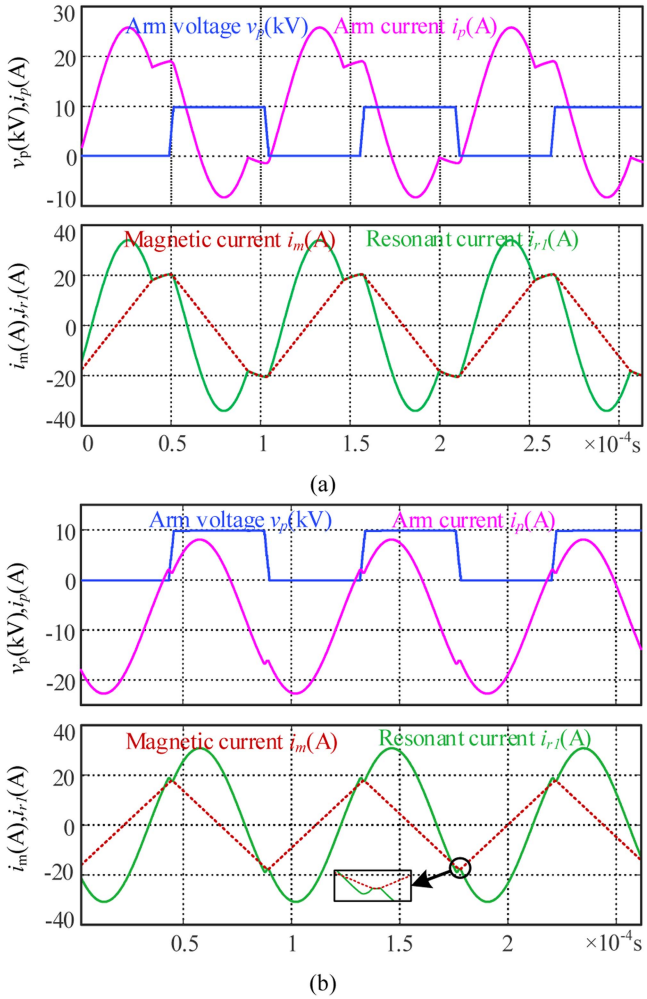

Fig. 15. Arm current and voltage under different load conditions. (a) 80 kW load condition. (b) −80 kW load condition.

behavior. In reverse mode, the dc bias of the arm current is negative, which presents a challenge for the upper devices of the SMs to achieve ZVS-ON. Therefore, maintaining a positive current in the arm at the SM switching time can overcome this problem, as shown in Fig. 15(b). During arm alternating, the current on the secondary side is reduced to zero, verifying the ZCS-OFF behavior of the device.

Fig. 16 shows the simulation waveforms of the BMMRDC during dynamic operation, the MVDC and LVDC terminal voltages are considered constant. The curves are the dynamic waveform of the LV side current, excitation current, and primary side current under the load condition from 80 kW to −80 kW. Thus, it is demonstrated that the power flow of the BMMRDC can be adjusted over a wide range. In addition, the converter has a fast dynamic response, allowing for power flow changes in less than 15 ms. The reason for the decrease in excitation current is the increase in operating frequency. However, this phenomenon would be detrimental to the acquisition of soft switching for the MMC unit.

Fig. 17 shows the voltage waveform of the bridge arm SM within the simulation model. The ripple voltage of the SM is

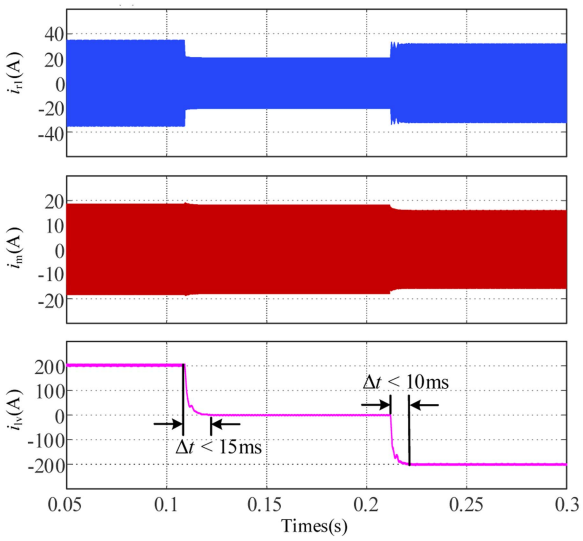

Fig. 16. Dynamic load shedding simulation waveform under continuous power conditions.

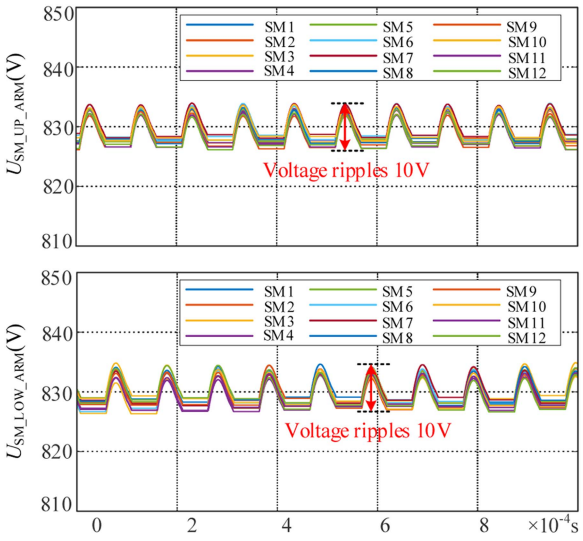

Fig. 17. Simulation waveform of SM voltage in the forward mode of two arms.

approximately 10 V, which represents a value less than 2% of the voltage rating.

B. Experimental Results

To validate the operational principles and power flow control strategies proposed in this article, a downscaled BMMRDC prototype was built for experimental verification, as shown in Fig. 18. The main parameters of the experimental prototype can be found in Table III. The dc supply voltage of the prototype on the MV side and the LV side are selected as 1 kV and 300 V, respectively, and the rated power is 4.5 kW. The prototype is employed to validate the feasibility of the proposed power control strategy, which is independent of voltage or power transfer level.

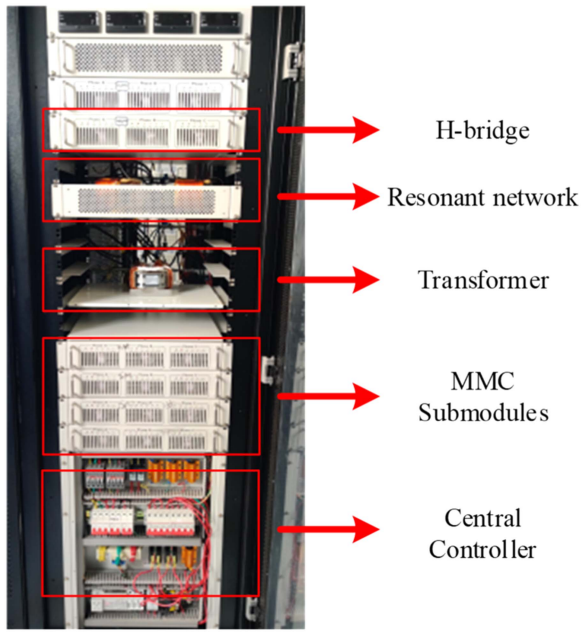

Fig. 18. 1 kV/4.5 kW laboratory prototype.

TABLE III
PARAMETERS OF EXPERIMENT

Parameters	Value
Medium terminal voltage V_m	1 kV
Low terminal voltage V_l	300 V
Bidirectional power P_{max}	±4.5 kW
MMC arm SM number N	4
SM capacitance C_{sm}	40 μF
Resonant ratio k	5
Transformer turns ratio n	2:1
Resonant frequency f_r	5 kHz
Resonant capacitor C_r	1.5 μF
Resonant inductance L_r	480 μH
Switching frequency f_s	3.5–5 kHz

The prototype is equipped with a protection device, which detects the voltage and current of the MV and LV sides through a sampling system, which could avoid potential damage to the conversion system in the event of faults. The effects of higher current stresses have been considered in the design, where the layout of components was optimized to reduce the overvoltage caused by the turn-ON and turn-OFF process of semiconductor devices. In addition, the steady operation of the power transfer can be maintained by adjusting the operating frequency of the converter in the event of voltage fluctuations on the dc bus.

The prototype uses the double sorting algorithm proposed in [23] to keep the SM voltages balanced. As gate drive signals with different phase shift angles have different charge and discharge capabilities, these drive signals are allocated to maintain voltage balance based on the sorting of the last period SM voltages.

Similar to the simulated waveforms shown in Fig. 19, the waveform illustrates the steady-state experimental waveforms of

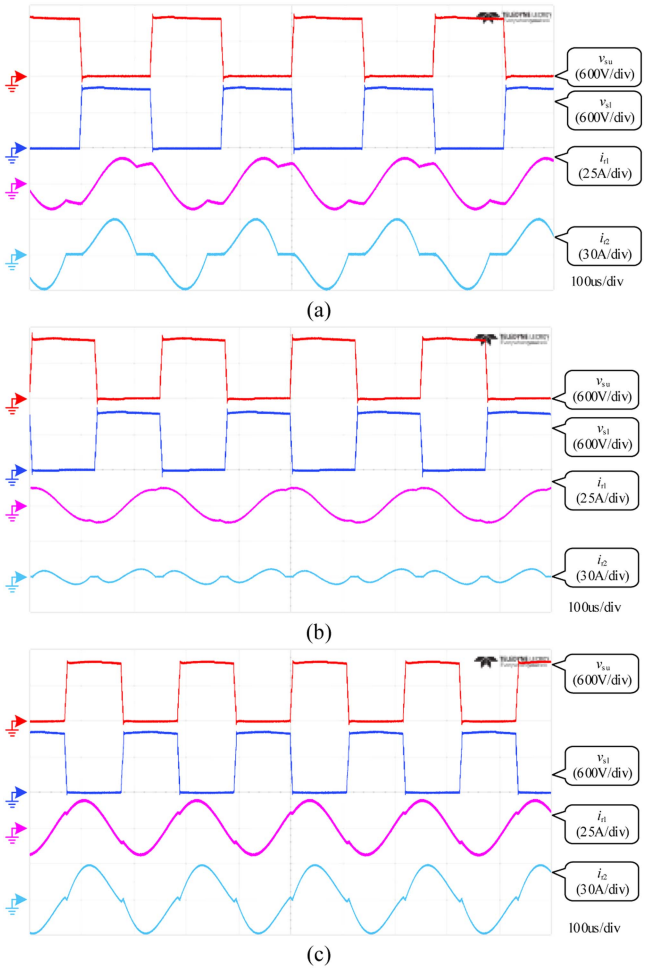

Fig. 19. Steady-state waveforms at different operating frequencies. (a) 3.5 kHz. (b) 4.0 kHz. (c) 4.7 kHz.

the converter in three different operating frequencies that are 3.5, 4.0, and 4.7 kHz. The waveform in Fig. 19(a) shows a behavior similar to a traditional *LLC* converter with no power backflow at an operating state of 4.5 kW. Besides, Fig. 19(b) shows the waveform under 0-kW conditions, where the resonant current is a triangular wave that feeds the excitation current. This indicates that the converter has the lowest efficiency. Finally, Fig. 19(c) shows the waveform at the −4.5 kW load condition, indicating that energy is predominantly transferred from the LV side to the MV side throughout the entire period.

The soft-switching behavior of the SM can be determined by analyzing the voltage-current relationship of the arm and the current on the secondary side reduced to zero can help the H-bridge achieve the ZCS. Fig. 20 shows the device of the SM can achieve the ZVS at the switching point under rated power conditions. Likewise, the device in the H-bridge has a soft-switching performance. As shown in Fig. 20(a) and (b), the devices can realize the ZVS and the ZCS in both forward and reverse modes, respectively. Optimizing the parameter design can reduce device losses and improve converter efficiency. Therefore, optimizing the parameter design can reduce device losses and improve converter efficiency.

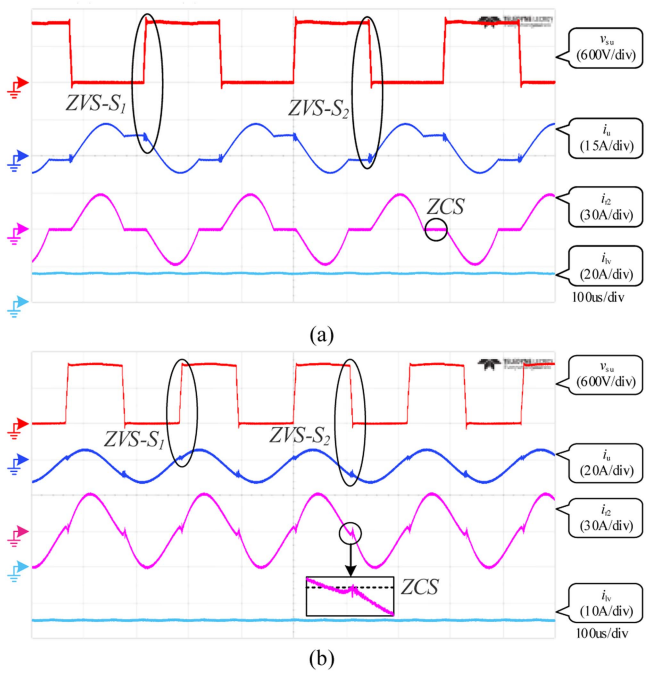

Fig. 20. Waveforms of soft switch about the BMMRDC in the experiment. (a) Operating in forward mode. (b) Operating in reverse mode.

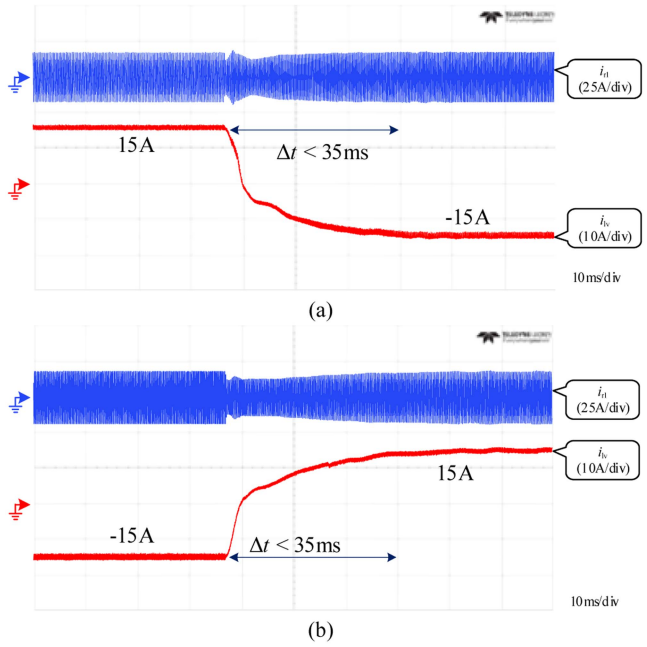

Fig. 21. Power step-change waveforms. (a) Power changes from 4.5 kW to −4.5 kW. (b) Power changes from −4.5 kW to 4.5 kW.

The experimental waveforms are highly consistent with the theoretical analysis. In the reverse operation mode, it is crucial to ensure that the secondary side current is zero at the end of the half cycle to prevent the soft switch on the secondary side from being lost.

Fig. 21 shows the dynamic behaviors of the proposed power flow control strategy. The waveforms are about the resonant

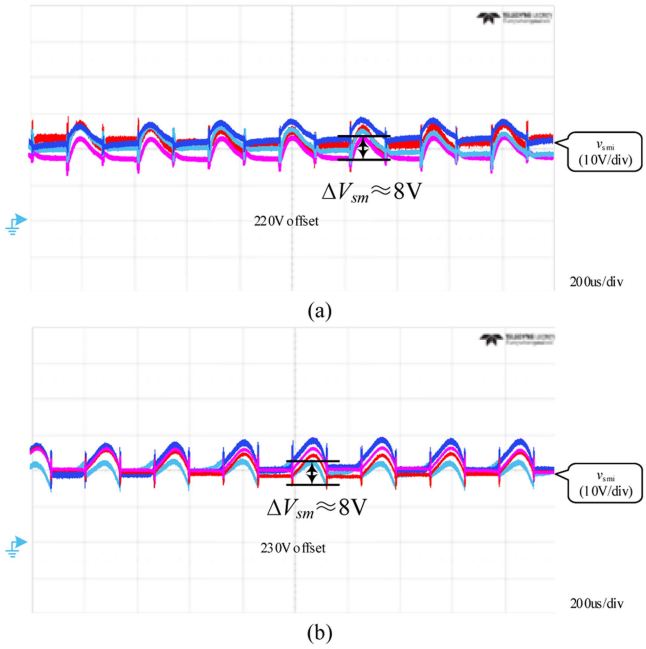

Fig. 22. Voltage waveform of SMs in forward mode. (a) Upper arm. (b) Lower arm.

current and the LV side current. Fig. 21(a) shows the dynamic waveform during the power condition switching from 4.5 kW to −4.5 kW in the closed-loop control. The transient time is less than 35 ms with better dynamic performance, which indicates that flexible power regulation can be achieved. In general, a response time in the millisecond range is sufficient for the converter to operate correctly. Likewise, the performance of the dynamic is satisfactory when the power condition changes from −4.5 kW to 4.5 kW, as shown in Fig. 21(b). This verifies that the proposed control strategy enables precise adjustment of power flow and has flexible power regulation ability.

Fig. 22 shows the SMs' capacitor voltages in forward mode, which can be sustained at approximately 250 V for each SM with the implementation of the balancing algorithm. It can be observed that there exists a difference among the capacitor voltages of the SMs, resulting from the slight capacitance discrepancy or measurement error. The ripple voltage is 8 V, which is 3% of the nominal capacitor voltage.

V. Conclusion

This article presents a power flow control strategy for a BMMRDC. The control strategy continuously and flexibly regulates the power of the BMMRDC, combining the benefits of both resonant unit and MMC. Considering the power shift angle to build the modeling of the gain about the BMMRDC, the maximum error is only 5.2% compared with the simulation results. It indicates that the model has a high accuracy. Therefore, the operating frequency of the converter is adjusted to affect the power shift angle φ to achieve power flow control. In addition, the soft-switching behavior of the devices with the proposed control strategy is analyzed. A wide range of device loss reduction can be achieved to improve the converter efficiency. In forward and reverse modes, the theoretically calculated efficiency is 98.2% and 97.9%, respectively. Finally, the proposed power flow strategy is validated through simulations and experiments using a downscaled prototype with 1 kV input and 300 V/4.5 kW output. The result shows that the proposed BMMRDC topology and control method have precise bidirectional power control capability and fast dynamic response, which is able to finish the dynamic process within 35 ms.

References

[1] S. Zhou, Z. Chen, D. Huang, and T. Lin, "Model prediction and rule based energy management strategy for a plug-in hybrid electric vehicle with hybrid energy storage system," *IEEE Trans. Power Electron.*, vol. 36, no. 5, pp. 5926–5940, May 2021.

[2] Z. Wang, Y. Zhang, S. You, H. Xiao, and M. Cheng, "An integrated power conversion system for electric traction and V2G operation in electric vehicles with a small film capacitor," *IEEE Trans. Power Electron.*, vol. 35, no. 5, pp. 5066–5077, May 2020.

[3] J. Yang, Z. He, H. Pang, and G. Tang, "The hybrid-cascaded dc–dc converters suitable for HVdc applications," *IEEE Trans. Power Electron.*, vol. 30, no. 10, pp. 5358–5363, Oct. 2015.

[4] X. Zhang, B. Wang, U. Manandhar, H. Beng Gooi, and G. Foo, "A model predictive current controlled bidirectional three-level dc/dc converter for hybrid energy storage system in dc microgrids," *IEEE Trans. Power Electron.*, vol. 34, no. 5, pp. 4025–4030, May 2019.

[5] Q. Song, B. Zhao, J. Li, and W. Liu, "An improved dc solid state transformer based on switched capacitor and multiple-phase-shift shoot-through modulation for integration of LVDC energy storage system and MVDC distribution grid," *IEEE Trans. Ind. Electron.*, vol. 65, no. 8, pp. 6719–6729, Aug. 2018.

[6] H. Akagi and R. Kitada, "Control and design of a modular multilevel cascade BTB system using bidirectional isolated dc/dc converters," *IEEE Trans. Power Electron.*, vol. 26, no. 9, pp. 2457–2464, Sep. 2011.

[7] M. Tabari and A. Yazdani, "Stability of a dc distribution system for power system integration of plug-in hybrid electric vehicles," *IEEE Trans. Smart Grid*, vol. 5, no. 5, pp. 2564–2573, Sep. 2014.

[8] B. Zhao, Q. Song, J. Li, W. Liu, G. Liu, and Y. Zhao, "High-frequency-link dc transformer based on switched capacitor for medium-voltage dc power distribution application," *IEEE Trans. Power Electron.*, vol. 31, no. 7, pp. 4766–4777, Jul. 2016.

[9] B. Li, S. Zhou, D. Xu, S. J. Finney, and B. W. Williams, "A hybrid modular multilevel converter for medium-voltage variable-speed motor drives," *IEEE Trans. Power Electron.*, vol. 32, no. 6, pp. 4619–4630, Jun. 2017.

[10] S. Zhao, Y. Chen, S. Cui, B. J. Mortimer, and R. W. De Doncker, "Three-port bidirectional operation scheme of modular-multilevel dc–dc converters interconnecting MVDC and LVDC grids," *IEEE Trans. Power Electron.*, vol. 36, no. 7, pp. 7342–7348, Jul. 2021.

[11] T. Jiang, J. Zhang, X. Wu, K. Sheng, and Y. Wang, "A bidirectional LLC resonant converter with automatic forward and backward mode transition," *IEEE Trans. Power Electron.*, vol. 30, no. 2, pp. 757–770, Feb. 2015.

[12] V. Karthikeyan and R. Gupta, "Multiple-input configuration of isolated bidirectional dc–dc converter for power flow control in combinational battery storage," *IEEE Trans. Ind. Inform.*, vol. 14, no. 1, pp. 2–11, Jan. 2018.

[13] F. Wang, G. Wang, A. Huang, W. Yu, and X. Ni, "Design and operation of A 3.6kV high performance solid state transformer based on 13kV SiC MOSFET and JBS diode," in *Proc. IEEE Energy Convers. Congr. Expo.*, 2014, pp. 4553–4560.

[14] D. Rothmund, T. Guillod, D. Bortis, and J. W. Kolar, "99.1% Efficient 10 kV SiC-based medium-voltage ZVS bidirectional single-phase PFC ac/dc stage," *IEEE J. Emerg. Sel. Topics Power Electron.*, vol. 7, no. 2, pp. 779–797, Jun. 2019.

[15] R. Chen et al., "Analysis and design for medium voltage Dual active bridge converter based on series-connected SiC MOSFETs," *IEEE Trans. Power Electron.*, vol. 38, no. 12, pp. 15620–15633, Dec. 2023.

[16] Z. Lu et al., "Medium voltage soft-switching DC/DC converter with series-connected SiC MOSFETs," *IEEE Trans. Power Electron.*, vol. 36, no. 2, pp. 1451–1462, Feb. 2021.

[17] C. Li et al., "High off-state impedance gate driver of SiC MOSFETs for crosstalk voltage elimination considering common-source inductance," *IEEE Trans. Power Electron.*, vol. 35, no. 3, pp. 2999–3011, Mar. 2020.
[18] A. Marzoughi, R. Burgos, and D. Boroyevich, "Active gate-driver with dv/dt controller for dynamic voltage balancing in series-connected SiC MOSFETs," *IEEE Trans. Ind. Electron.*, vol. 66, no. 4, pp. 2488–2498, Apr. 2019.
[19] C. Li, S. Chen, H. Luo, C. Li, W. Li, and X. He, "A modified RC snubber with coupled inductor for active voltage balancing of series-connected SiC MOSFETs," *IEEE Trans. Power Electron.*, vol. 36, no. 10, pp. 11208–11220, Oct. 2021.
[20] G. Zheng, Y. Chen, and Y. Kang, "Trapezoidal current modulation for a compact dc modular multilevel converter with ZVS of submodules and ZCS of voltage-balancing circuits," *IEEE Trans. Power Electron.*, vol. 36, no. 10, pp. 10986–10992, Oct. 2021.
[21] P. A. Gray, P. W. Lehn, and N. Yakop, "A modular multilevel dc–dc converter with flying capacitor converter like properties," *IEEE Trans. Ind. Electron.*, vol. 69, no. 7, pp. 6774–6783, Jul. 2022.
[22] H. Liu, M. S. A. Dahidah, J. Yu, R. T. Naayagi, and M. Armstrong, "Design and control of unidirectional dc–dc modular multilevel converter for offshore dc collection point: Theoretical analysis and experimental validation," *IEEE Trans. Power Electron.*, vol. 34, no. 6, pp. 5191–5208, Jun. 2019.
[23] S. Shao, M. Jiang, J. Zhang, and X. Wu, "A capacitor voltage balancing method for a modular multilevel dc transformer for dc distribution system," *IEEE Trans. Power Electron.*, vol. 33, no. 4, pp. 3002–3011, Apr. 2018.
[24] J. Zhang, Z. Wang, and S. Shao, "A three-phase modular multilevel dc–dc converter for power electronic transformer applications," *IEEE J. Emerg. Sel. Topics Power Electron.*, vol. 5, no. 1, pp. 140–150, Mar. 2017.
[25] Y. Qiao, X. Zhang, X. Xiang, X. Yang, and T. C. Green, "Trapezoidal current modulation for bidirectional high-step-ratio modular dc–dc converters," *IEEE Trans. Power Electron.*, vol. 35, no. 4, pp. 3402–3415, Apr. 2020.
[26] J. Sheng et al., "High-efficient operation for modular multilevel resonant dc–dc converters in medium voltage applications with wide input range and wide load condition," *IEEE Trans. Power Electron.*, vol. 38, no. 10, pp. 12180–12194, Oct. 2023.
[27] J. Sheng et al., "Control optimization of modular multilevel resonant dc converters for wide-input-range MVdc to LVdc applications," *IEEE Trans. Power Electron.*, vol. 37, no. 5, pp. 5284–5298, May 2022.
[28] S. Shao et al., "A modular multilevel resonant dc–dc converter," *IEEE Trans. Power Electron.*, vol. 35, no. 8, pp. 7921–7932, Aug. 2020.
[29] H. Jin, W. Chen, K. Hou, S. Shao, L. Shu, and R. Li, "A sharing-branch modular multilevel dc transformer with wide voltage range regulation for dc distribution grids," *IEEE Trans. Power Electron.*, vol. 37, no. 5, pp. 5714–5730, May 2022.
[30] H. Jin, W. Chen, S. Shao, and L. Shu, "A quasi-square-wave modular multilevel resonant dc/dc converter with ZCS and current-shaping capacity for high step-ratio application," *IEEE Trans. Power Electron.*, vol. 38, no. 1, pp. 548–565, Jan. 2023.
[31] V. Vorperian, "Quasi-square-wave converters: Topologies and analysis," *IEEE Trans. Power Electron.*, vol. 3, no. 2, pp. 183–191, Apr. 1988.
[32] Y. Wei, Q. Luo, X. Du, N. Altin, A. Nasiri, and J. M. Alonso, "A dual half-bridge LLC resonant converter with magnetic control for battery charger application," *IEEE Trans. Power Electron.*, vol. 35, no. 2, pp. 2196–2207, Feb. 2020.
[33] T. H. Nguyen and D.-C. Lee, "Deterioration monitoring of dc-link capacitors in ac machine drives by current injection," *IEEE Trans. Power Electron.*, vol. 30, no. 3, pp. 1126–1130, Mar. 2015.
[34] R. Li, W. Chen, S. Shao, H. Jin, L. Shu, and S. Gao, "A novel hybrid dc transformer combining modular multilevel converter structure and series-connected semiconductor switches," *IEEE Trans. Power Electron.*, vol. 37, no. 5, pp. 5699–5713, May 2022.

Boliang Li was born in Shannxi, China, in 1998. He received the B.S. degree in electrical engineering from South China University of Technology, Guangzhou, China, in 2021, and the M.S. degree in electrical engineering from Xi'an Jiaotong University, Xi'an, China, in 2024.

His current research focuses on the control of medium-voltage high-power converters.

Jing Sheng (Member, IEEE) received the B.S. and Ph.D. degrees in electrical engineering from the College of Electrical Engineering, Zhejiang University, Hangzhou, China, in 2017 and 2023, respectively.

He is currently a Postdoctoral Researcher with the College of Electrical Engineering, Zhejiang University. From May 2021 to May 2022, he was a visiting Ph.D. student with Power Electronics Laboratory, École Polytechnique Fédérale de Lausanne, Lausanne, Switzerland. His research interests include modulation and control of medium-voltage multilevel converters.

Long Xu was born in Shandong, China, in 2000. He received the B.S. degree in electrical engineering from the College of Electrical and Information Engineering, Hunan University, Changsha, China, in 2022. He is currently working toward the M.S. degree in electrical engineering with the College of Electrical Engineering, Zhejiang University, Hangzhou, China.

His research interests include the analysis and control of modular multilevel converters.

Tianling Shi (Member, IEEE) received the B.Sc. degree in electrical engineering and automation from the School of Electrical and Information Engineering, Jiangsu University, Zhenjiang, China, in 2018. He is currently working toward the Ph.D. degree in electrical engineering with Shanghai University, Shanghai, China, and the University of Technology Sydney, Sydney, NSW, Australia, through the Collaborative Doctoral Research Degree Program.

From 2021 to 2023, he was a Visiting Researcher with the College of Electrical Engineering, Zhejiang University, Zhejiang, China. His research interests include the control and protection of dc microgrids.

Shiyuan Fan received the B.Sc. degree in electrical engineering and its automation from North China Electric Power University, Beijing, China in 2018, and the Ph.D. degree in electrical engineering from Zhejiang University, Hangzhou, China, in 2023.

In 2018, she was a visiting student with the University of Milwaukee-Wisconsin, Milwaukee WI, USA. From November 2021 to July 2022, she was a visiting scholar with Imperial College London, London, U.K. She is currently a postdoctoral researcher with the University of Tennessee, Knoxville, Knoxville, TN, USA. Her research interests include modular multilevel converters, V2G, and grid resilience.

Xin Xiang (Member, IEEE) received the B.Sc. degree from the Harbin Institute of Technology, Harbin, China, in 2011, the M.Sc. degree from Zhejiang University, Hangzhou, China, in 2014, and the Ph.D. degree from the Imperial College London, London, U.K., in 2018, all in electrical and electronic engineering.

From 2018 to 2020, he was a Research Associate with Imperial College London, London, U.K. He is currently a tenure-track Associate Professor with the College of Electrical Engineering, Zhejiang University. His research interests include the analysis and control of power electronics converters for power system applications.

Dr. Xiang was the recipient of the Eryl Cadwaladr Davies Prize for the Best Ph.D. Thesis of Electrical and Electronic Engineering Department, Imperial College London, and the Best Ph.D. Thesis Award from IEEE Power Electronics Society U.K. and Ireland Chapter.

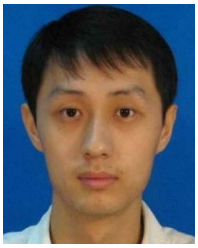

Xiaotian Zhang (Senior Member, IEEE) was born in Xi'an, China, in 1983. He received the B.S. (honors) and M.S. degrees in electrical engineering from Jiaotong University, Xi'an, China, in 2006 and 2009, respectively, and the Ph.D. degree (honors) in electrical engineering and electronics from the University of Liverpool, Liverpool, U.K., in 2012.

Until 2015, he was with the Department of Electrical Engineering, Imperial College London, London, U.K. He is currently an Associate Professor with the Department of Electrical Engineering, Xi'an Jiaotong University, Xi'an, China. His research interests include control and design of HVdc converters.

Wuhua Li (Senior Member, IEEE) received the B.Sc. and Ph.D. degrees in power electronics and electrical engineering from Zhejiang University, Hangzhou, China, in 2002 and 2008, respectively.

From 2004 to 2005, he was a Research Intern, and from 2007 to 2008, a Research Assistant with GE Global Research Center, Shanghai, China.

From 2008 to 2010, he was a postdoctortoral researcher with the College of Electrical Engineering, Zhejiang University, where he was promoted to Associate Professor in 2010. From 2010 to 2011, he was a Postdoctoral Fellow with the Department of Electrical and Computer Engineering, Ryerson University, Toronto, ON, Canada. Since 2013, he has been a Full Professor with Zhejiang University. He is currently the Executive Deputy Director of the National Specialty Laboratory for Power Electronics and the Vice Director of the Power Electronics Research Institute, Zhejiang University. He has authored or coauthored more than 300 peer-reviewed technical papers and holds over 50 issued/pending patents. His research interests include power devices, converter topologies, and advanced controls for high-power energy conversion systems.

Dr. Li is currently an Associate Editor for the *Journal of Emerging and Selected Topics in Power Electronics*, *IET Power Electronics*, *CSEE Journal of Power and Energy Systems*, *CPSS Transactions on Power Electronics and Applications,* and *Proceedings of the Chinese Society for Electrical Engineering*, a Guest Editor for *IET Renewable Power Generation* for Special Issue "DC and HVDC system technologies," and a Member of Editorial Board for *Journal of Modern Power System and Clean Energy*. He was the recipient of the 2012 Delta Young Scholar from Delta Environmental & Educational Foundation, the 2012 Outstanding Young Scholar from the National Science Foundation of China, the 2013 Chief Youth Scientist of the National 973 Program, 2014 Young Top-Notch Scholar of the National Ten Thousand Talent Program, and 2019 Distinguished Young Scholar from National Science Foundation of China, due to his excellent teaching and research contributions. He was also the recipient of one National Natural Science Award and four Scientific and Technological Achievement Awards from the Zhejiang Provincial Government and the State Educational Ministry of China. Since 2014, he has been the Most Cited Chinese Researcher by Elsevier.